Electronic Supplementary Information for

Electrochemical Hydrogen Formation Catalysed by a Pd_8 String

Tomoaki Tanase,* Kanako Nakamae, Haruka Miyano, Yoshimi Fujisawa, Yasuyuki Ura, and Takayuki Nakajima

Department of Chemistry, Faculty of Science, Nara Women's University, Kitauoya-nishi-machi, Nara 630-8506, Japan.

dpmppm)$_2$(CH$_3$CN)$_2$]$^{3+}$ (**4$_{opt}$**), with LANL2DZ (for Pd), 6-311+G(d,p) (for hydride H), and 6-31G(d) (for others) basis sets, and IEFPCM (CH$_3$CN). The C–H hydrogen atoms are omitted for clarity. Pd (violet), P (orange), N (blue), C (gray), and hydride H (pink).

Figure S3. UV-vis-NIR spectral changes in CH$_3$CN for titration of [Pd$_8$(*meso*-dpmppm)$_4$(CH$_3$CN)$_2$](BF$_4$)$_4$ (**1**) with successive addition of HBF$_4$ (portions of 0.1 eq.) at room temperature, forming **4** with the band maximum at 568 nm.

Figure S4. ESI mass spectra of **4** in CH$_3$CN at room temperature.

Figure S5. ^{31}P{^{1}H} NMR spectral changes in CD$_3$CN for the reactions of [Pd$_8$(*meso*-dpmppm)$_4$(CH$_3$CN)$_2$](BF$_4$)$_4$ (**1**) with 0–4, eq. of HBF$_4$, showing the four resonances corresponding to **4**.

Figure S6. (a) ^{1}H{^{31}P} NMR of **1**, (b) ^{1}H{^{31}P}and (c) ^{31}P{^{1}H} NMR spectra of **4** (generated from **1** with excess HBF$_4$ in situ) in CD$_3$CN at room temperature.

Figure S7. ^{31}P–^{31}P COSY (a) and ^{1}H–^{31}P HMBC (b) NMR spectra (121 MHz) of **4** (generated from **1** with excess HBF$_4$ in situ) in CD$_3$CN at room temperature.

Figure S8. UV-vis absorption spectrum of **5** in CD$_3$CN at room temperature.

Figure S9. ESI mass spectra of **5** in CH$_3$CN at room temperature.

Figure S10. ^{1}H{^{31}P}, ^{31}P{^{1}H}, and ^{31}P–^{31}P COSY NMR spectra of **5** in CD$_3$CN at room temperature.

Figure S11. ^{31}P{^{1}H} NMR spectral changes of (a) **1**, (b) after addition of HBF$_4$·Et$_2$O (2 eq.), generating **4**, and (c) after further addition of Cp$_2$Co (4 eq.), restoring **1**, in CD$_3$CN at room temperature.

Figure S12. MO diagrams for [Pd$_4$(H)(*meso*-dpmppm)$_2$(CH$_3$CN)$_2$]$^{3+}$ (**4$_{opt}$**) derived from DFT calculations with B3LYP-D3BJ functionals and LANL2DZ (for Pd), 6-311+G(d,p) (for hydride H), and 6-31G(d) (for others), and IEFPCM(CH$_3$CN).

Figure S13. Cyclic voltammograms for 1 mM of **1** without HBF$_4$ (red line), with 2 eq. of HBF$_4$ (black line), and with 5 eq. of HBF$_4$ (blue line). Measured at room temperature with scan rate of 100 mV/s in CH$_3$CN containing 0.1 M [Bu$_4$N][BF$_4$].

Figure S14. Cyclic voltammograms for 1 mM of **1** without HBF$_4$ (red line), with 2−10 eq. of HBF$_4$ (black and blue dotted lines), measured at room temperature with scan rate of 100 mV/s in CH$_3$CN containing 0.1 M [^{n}Bu$_4$N][BF$_4$].

Figure S15. (a) Cyclic voltammograms for 1 mM of **1** without HBF_4 (red line), with 10–100 eq. of HBF_4, measured at room temperature with scan rate of 100 mV/s in CH_3CN containing 0.1 M [$^{n}Bu_4N$][BF_4] (left). A plot of I_{cat}/I_p vs $[H^+]^{1/2}$ (right). (b) CVs without **1** under the same conditions with HBF_4 (0–60 eq.), showing significantly weak reduction currents in comparison with those with **1**(a).

Figure S16. Cyclic voltammograms of repeating scans with (a) CMGCE/Nafion-**3**, (b) CMGCE/Nafion-**1**, and (c) CMGCE/Nafion, measured at room temperature with scan rate of 100 mV/s in CH_3CN containing 0.1 M [$^{n}Bu_4N$][BF_4].

Figure S17. Cyclic voltammogram with CMGCE/Nafion-**3**, , measured at room temperature with scan rate of 100 mV/s in CH_3CN containing 0.1 M [$^{n}Bu_4N$][BF_4] (left), and those with various scan rates from 50 to 1000 mV/s-1, and (c) a plot of I_{pc} vs scan rate v/mVs^{-1}.

Figure S18. Cyclic voltammograms with CMGCE/Nafion-**3**, in the presence of excess amounts of HBF4 (0-100 x 10^5 eq. vs **3**), measured at room temperature with scan rate of 100 mV/s in CH_3CN containing 0.1 M [$^{n}Bu_4N$][BF_4], and a plot of i_{cat}/i_p vs $([H^+]^{1/2})/M^{-0.5}$.

Figure S19. IR spectrum of $[Pd_4(H)($*meso*-dpmppm$)_2(CH_3CN)_2](BF_4)_3$ (**4**) as KBr pellet.

Table S6. Cartesian coordinates of the DFT optimized structure $\mathbf{4_{opt}}$.

Materials and Methods

All procedures were carried out under nitrogen atmosphere by using standard Schlenk techniques or in a glove box. Solvents were dried by standard procedures and freshly distilled prior to use. Fullerenes Nafion© (2.5% dispersion) was purchased from Sigma-Aldrich Co. Ltd. Other reagents were of the best commercial grade and no further purifications were performed. The tetraphosphines *meso*-bis[(diphenylphosphinomethyl)phenylphosphino]methane (dpmppm), and the octapalladium complexes **1**, **2**, and **3** were prepared by the method already reported.[S1-S5] ^{1}H NMR spectra were recorded on a Bruker AV-300N spectrometer at 300 MHz; frequencies are referenced to the residual resonances of the deuterated solvent. $^{31}P\{^{1}H\}$ NMR spectra were recorded on the same instruments at 121 MHz with chemical shifts being calibrated to 85 % H_3PO_4 as an external reference. ^{31}P-^{31}P COSY and ^{1}H-^{31}P HMBC NMR measurements were also performed on the same instrument. Electronic absorption spectra were recorded on Agilent 8453 and JASCO UV600 spectrophotometers. IR spectra of solid samples as KBr disks were recorded on a JASCO FT/IR 410 spectrophotometer at ambient temperature. ESI-TOF mass spectra were recorded on a JEOL JMS-T100LC high-resolution mass spectrometer equipped with an ion spray interface with a positive detection mode in the range of *m/z* 100–3000. The sprayer was held at a potential of +1.0 kV, and the compressed N_2 was employed to assist liquid nebulization (37 ºC). Orifice potential was maintained at +40 V (45 ºC). Electrochemical measurements were performed with a HOKUTO-Denko HZ-3000 system. [$^{n}Bu_4N$][PF_6] was used as supporting electrolyte, which was recrystallized from ethanol before in use. Cyclic voltammetry experiments were carried with ca. 1 mM acetonitrile solutions of the samples containing 0.1 M [$^{n}Bu_4N$][BF_4], by using a standard three-electrode cell consisting of a Ag/$AgPF_6$ reference electrode, platinum wire as counter-electrode, and glassy carbon electrode (5 mmϕ) as working electrode. The chronocoulometry was carried out with the same system by using a Pt mesh or Hg pool electrode. The potential data were referenced to the Fc/Fc^{+} half potential (as 0 V) measured with the same system (Fc = $Fe(\eta^5\text{-}C_5H_5)_2$).

Preparation of $[Pd_4(H)(\textit{meso}\text{-dpmppm})_2(CH_3CN)_2](BF_4)_3$ (4): To an acetonitrile solution (2 mL) of $[Pd_8(\textit{meso}\text{-dpmppm})_4(CH_3CN)_2](BF_4)_4$ (**1**) (26.5 mg, 6.98 μmol) was added $HBF_4{\cdot}Et_2O$ (4.52 mg, 27.9 μmol) with dichloromethane (1 mL), and the reaction mixture was stirred for 1 h at room temperature. The solvent was evaporated under reduced pressure to ca. 1 mL. After careful addition of diethyl ether (ca. 2 mL), the solution was allowed to stand at room temperature for 12 h to yield violet microcrystals of **4**$\cdot 1.5CH_2Cl_2$, which were collected by filtration, washed with diethyl ether, and dried under vacuum (21.7 mg, 72% vs **1**). Anal. Calc. for $C_{83.5}H_{82}N_2B_3F_{12}Cl_3P_8Pd_4$: C, 46.56; H, 3.84; N, 1.30 %; Found: C, 46.47; H, 3.84; N, 1.26 %. IR (KBr): ν), 2207 (w), 1484 (m), 1437 (s), 1364 (m), 1309 (w), 1281 (w), 1188 (m), 1123 (s), 1084 (s), 999 (s), 925 (w), 847 (w), 786 (s), 741 (s), 692 (s), 533 (m), 512 (m), 481 (m) cm^{-1}. UV-vis (in CH_3CN at r.t.): λ_{max} (log ε) 568 nm. $^1H\{^{31}P\}$ NMR (in CD_3CN, at r.t.): δ 7.69—5.96 (Ph, 64H), 4.25 (d, J_{HH} = 14 Hz, 2H, CH_2), 4.06 (d, J_{HH} = 14 Hz, 2H, CH_2), 3.95 (d, J_{HH} = 14 Hz, 2H, CH_2), 3.85 (d, J_{HH} = 14 Hz, 2H, CH_2), 3.60 (d, J_{HH} = 14 Hz, 2H, CH_2), 3.56 (d, J_{HH} = 14 Hz, 2H, CH_2), −12.34 (s, hydride). $^{31}P\{^1H\}$ NMR (in CD_3CN at r.t.): δ 15.8 (2P), −2.1 (2P), −4.5 (2P), −15.2 (2P). ESI-MS (in CH_3CN): *m/z* 561.0440 (*z*3, $[Pd_4H(dpmppm)_2]^{3+}$ (560.9935)), 574.7138 (*z*3, $[Pd_4H(dpmppm)_2(CH_3CN)]^{3+}$ (574.6691)), 588.7336 (*z*3, $[Pd_4H(dpmppm)_2(CH_3CN)_2]^{3+}$ (588.6781)), 905.5975 (*z*2, $\{[Pd_4H(dpmppm)_2]BF_4\}^{2+}$ (905.5055)), 1898.2196 (*z*1, $\{[Pd_4H(dpmppm)_2](BF_4)_2\}^{+}$ (1898.0146)).

Preparation of $[Pd_4(\eta^2\text{-tcne})(\textit{meso}\text{-dpmppm})_2(CH_3CN)](BF_4)_2$ (5): To an acetonitrile solution (2 mL) of $[Pd_8(\textit{meso}\text{-dpmppm})_4(XylNC)_2](BF_4)_4$ (**2**) (32.6 mg, 8.60 μmol) was added tcne (tetracyanoethene) (2.20 mg, 17.2 μmol) with dichloromethane (1 mL), and the reaction mixture was stirred for 1 h at room temperature. The solvent was evaporated under reduced pressure to ca. 1 mL. After careful addition of diethyl ether (ca. 2 mL), the solution was allowed to stand at room temperature for 12 h to yield violet crystals of **5**$\cdot 1.5CH_2Cl_2$, which were collected by filtration, washed with diethyl ether, and dried under vacuum (26.5 mg, 76% vs **1**). Anal. Calc. for $C_{87.5}H_{78}N_5B_2F_8P_8Cl_3Pd_4$: C, 48.81; H, 3.65; N, 3.25 %; Found: C, 48.84; H, 3.90; N, 3.18 %. IR (KBr): ν 2217 (s), 1483 (s), 1436 (s), 1366 (s), 1336 (w), 1309 (m), 1279 (w), 1218 (w), 1189 (m), 1160 (m), 1123 (s), 1084 (s), 999 (s), 920 (w), 845 (w), 792 (s), 741 (s), 692 (s), 616 (w), 513 (s), 480 (s), 427 (s) cm^{-1}. UV-vis/NIR (in CH_3CN at r.t.): λ_{max} (log ε) 560 (4.96) nm. ^1H NMR (in CD_3CN, at r.t.): δ 7.82–6.43 (Ph, 60H), 4.17 (br, 4H, CH_2), 3.83 (br, 4H, CH_2), 3.68 (br, 4H, CH_2). $^{31}P\{^1H\}$ NMR (in CD_3CN at r.t.): δ 14.4 (2P), −1.4 (2P), −5.8 (2P), −13.6 (2P). ESI-MS (in CH_3CN): *m*/*z* 841.1231 (*z*2, $[Pd_4(dpmppm)_2]^{2+}$ (840.9864)), 905.1410 (*z*2, $[Pd_4(dpmppm)_2(tcne)]^{2+}$ (904.9926)), 1897.3161 (*z*1, $\{[Pd_4(dpmppm)_2(tcne)](BF_4)\}^+$ (1896.9889)). The plate shaped crystals of **5**·$4CH_3CN$ suitable for X-ray crystallography were obtained by recrystallization from CH_3CN/Et_2O mixed solvent in refrigerator .

Preparation of chemically modified glassy carbon electrode (CMGCE) with [Pd_8(*meso*-dpmppm)$_2$(2,3,5,6-tetramethylphenyl-1,4-bisisocyanide (BI))](BF_4)$_4$ (3) (CMGCE/Nf-3): To an acetonitrile solution (0.5 mL) containing $[Pd_8$(*meso*-dpmppm)$_4(CH_3CN)_2](BF_4)_4$ (**1**) and 2,3,5,6-tetramethyl-1,4-bisisocyanide (BI), forming 17 mM solution of $\{[Pd_8$(*meso*-dpmppm)$_4$(BI)]$(BF_4)_4\}_n$ (**3**),[S6] was added 2.5% Nafion dispersion solution in in ^{i}PrOH/EtOH (1:1 v/v, 500 μL). The mixture was quickly stirred to afford a stock solution which was used in preparation of chemically modified glassy carbon electrode (CMGCE). A 20 μL portion of the stock solution was casted on the surface of glassy carbon electrode (5 mm*ϕ*), which was dried under nitrogen for 30 min to give a CMGCE coated with Nafion film containing **3** (CMGCE/Nf-**3**). Then, the electrodes was electrochemically swept (ca. 40 cycles with a scan rate of 100 mV/s) in a potential window of −1.8 V to 0.8 V (vs Fc/Fc^+) until peak currents for the redox process at $E_{1/2}$ = −1.24 V became constant in 0.1 M CH_3CN solution of $[^nBu_4N][BF_4]$, according to the reported procedures.[S7]

X-ray Crystallographic Analysis. The needle crystal of **5**·4CH_3CN was quickly coated with Paratone N oil and mounted on top of a loop fiber at room temperature. Reflection data were collected at low temperature with a Rigaku VariMax Mo/Saturn CCD diffractometer equipped with graphite-monochromated confocal Mo Kα radiation using a rotating-anode X-ray generator RA-Micro7 (50 kV, 24 mA). Crystal and experimental data are summarized in Tables S1. All data were collected at −120 °C and a total of 1080 oscillation images, covering a whole sphere of 6° < 2θ < 55°, were corrected by the ω–scan method (−62° < ω < 118°) with $\Delta\omega$ of 0.50°. The crystal-to-detector (70 × 70 mm) distance was set at 60 mm. The data were processed using the *Crystal Clear 1.3.5* program (Rigaku/MSC)[S8] and corrected for Lorentz–polarization and absorption effects[S9]. The structures of complexes were solved by direct methods with *SHELXS-97*[S10] and were refined on F^2 with full-matrix least-squares techniques with *SHELXL-97*[S13] using *Crystal Structure 3.8* package[S12]. All non-hydrogen atoms were refined with anisotropic thermal parameters, and the C−H hydrogen atoms were calculated at ideal positions and refined with riding models. All calculations were carried out on a Windows PC with *Crystal Structure 3.8* package[S12].

CCDC 2105298 (**5**) contains the supplementary crystallographic data for this paper. These data can be obtained free of charge via www.ccdc.cam.ac.uk/data_request/cif, or by emailing data_request@ccdc.cam.ac.uk, or by contacting The Cambridge Crystallographic Data Centre, 12 Union Road, Cambridge CB2 1EZ, UK; fax +44 1223 336033.

Theoretical Calculations: DFT optimization of $[Pd_4(H)(\textit{meso}\text{-dpmppm})_2(CH_3CN)_2]^{3+}$ (**4**$_{\mathbf{opt}}$) was performed by using B3LYP(-D3BJ)[S14-S18] functionals with LANL2DZ[S19,20] (for Pd), &-311+G(d,p) (for hydride H), and 6-31G(d) (for others) basis sets, and solvent effects considered by IEFPCM(CH_3CN) mode. The initial coordinates are derived by modification of the crystal structure of **5**. The optimized structure was verified that they did not have any negative frequencies, which indicated the Pd–H stretching vibration energy of 2226 cm^{-1}, while only a weak peak was observed at 2207 cm^{-1} in the IR spectrum (Figure S19). TD–DFT calculations[S21] and NBO analyses[S22-24] were carried out with same functionals. All calculations were carried out using Research Center for Computational Science, Okazaki, Japan with *Gaussian 09/16* program packages.[S25]

Supporting References

S1. Y. Takumura, H. Takenaka. T. Nakajima, T. Tanase, *Angew. Chem. Int. Ed.* **2009**, *48*, 2157–2161.

S2. T. Tanase, R. Otaki, T. Nishida, H. Takenaka, Y. Takemura, B. Kure, T. Nakajima, Y. Kitagawa, T. Tsubomura, *Chem. Eur. J.* **2014**, *20*, 1577–1596.

S3. K. Nakamae, Y. Takemura, B. Kure, T. Nakajima, Y. Kitagawa, T. Tanase, *Angew. Chem., Int. Ed.* **2015**, *54*, 1016–1021.

S4. T. Tanase, K. Morita, R. Otaki, K. Yamamoto, Y. Kaneko, K. Nakamae, B. Kure, T. Nakajima, *Chem. Eur. J.* **2017**, *23*, 524–528.

S5. T. Tanase, K. Nakamae, S. Hayashi, A. Okue, T. Nishida, Y. Ura, Y. Kitagawa, T. Nakajima, *Inorg. Chem.* **2021**, *60*, 3259–3273.

S6. T. Tanase, K. Nakamae, H. Miyano, Y. Ura, Y. Kitagawa, S. Yada, T. Yoshimura, T. Nakajima, *Chem. Eur. J.* **2021**, *27*, 12078-12103.

S7. A. S. Kumar, T. Tanase, M. Iida, *Langmuir* **2007**, *23*, 391-394.

S8. *Crystal Clear, version 1.3.5; Operating software for the CCD detector system*, Rigaku and Molecular Structure Corp., Tokyo, Japan and The Woodlands, Texas, 2003.

S9. R. Jacobson, *REQAB*; Molecular Structure Corporation: The Woodlands, Texas, USA, 1998.

S10. G. M. Sheldrick, *SHELXS-97: Program for the Solution of Crystal Structures.* University of Göttingen, Göttingen, Germany, 1996。

S11. G. M. Sheldrick, *SHELXL-97: Program for the Refinement of Crystal Structures.* University of Göttingen, Göttingen, Germany, 1996.

S12. *Crystal Structure 3.8 and 4.0*: *Crystal Structure Analysis Package*, Rigaku Corporation

(2000-2010). Tokyo 196-8666, Japan.

S13. A. L. Spek, *Acta Crystallogr.* **2009**, *D65*, 148–155.

S14. A. D. Becke, *Phys. Rev. A* **1988**, *38*, 3098–3100.

S15. C. Lee, W. Yang, R. G. Parr, *Phys. Rev. B* **1988**, *37*, 785–789.

S16. B. Miehlich, A. Savin, H. Stoll, H. Preuss, *Chem. Phys. Lett.* **1989**, *157*, 200–206.

S17. A. D. Becke, *J. Chem. Phys.* **1993**, *98*, 5648–5652.

S18. (a) S. Grimme, J. Antony, S. Ehrlich, H. Krieg, *J. Chem. Phys*., **2010**, ***132***, 154104. (b) S. Grimme, S. Ehrlich and L. Goerigk, *J. Comput. Chem.*, **2011**, *32*, 1456–1465.

S19. P. J. Hay, W. R. Wadt, *J. Chem. Phys.* **1985**, *82*, 299–310.

S20. L. E. Roy, P. J. Hay, R. L. J. Martin, *Chem. Theory Comput.* **2008**, *4*, 1029–1031.

S21. M. E. Casida, C. Jamorski, K. C. Casida, D. R. Salahub, *J. Chem. Phys.* **1998**, *108*, 4439–4449.

S22. A. E. Reed, L. A. Curtiss, F. Weinhold, *Chem. Rev.* **1988**, *88*, 899–926.

S23. *NBO 6.0*; E. D. Glendening, J. K. Badenhoop, A. E. Reed, J. E. Carpenter, J. A. Bohmann, C. Morales, C. R. MLandis, F. Weinhold, Theoretical Chemistry Institute, University of Wisconsin: Madison, WI, 2013.

S24. K. B. Wiberg, *Tetrahedron* **1968**, *24*, 1083–1096.

S25. Gaussian 09 and 16, Revision C.01, M. J. Frisch, G. W. Trucks, H. B. Schlegel, G. E. Scuseria, M. A. Robb, J. R. Cheeseman, G. Scalmani, V. Barone, B. Mennucci, G. A. Petersson, H. Nakatsuji, M. Caricato, X. Li, H. P. Hratchian, A. F. Izmaylov, J. Bloino, G. Zheng, J. L. Sonnenberg, M. Hada, M. Ehara, K. Toyota, R. Fukuda, J. Hasegawa, M. Ishida, T. Nakajima, Y. Honda, O. Kitao, H. Nakai, T. Vreven, J. A. Montgomery, Jr., J. E. Peralta, F. Ogliaro, M. Bearpark, J. J. Heyd, E. Brothers, K. N. Kudin, V. N. Staroverov, R. Kobayashi, J. Normand, K. Raghavachari, A. Rendell, J. C. Burant, S. S. Iyengar, J. Tomasi, M. Cossi, N. Rega, J. M. Millam, M. Klene, J. E. Knox, J. B. Cross, V. Bakken, C. Adamo, J. Jaramillo, R. Gomperts, R. E. Stratmann, O. Yazyev, A. J. Austin, R. Cammi, C. Pomelli, J. W. Ochterski, R. L. Martin, K. Morokuma, V. G. Zakrzewski, G. A. Voth, P. Salvador, J. J. Dannenberg, S. Dapprich, A. D. Daniels, Ö. Farkas, J. B. Foresman, J. V. Ortiz, J. Cioslowski, D. J. Fox, Gaussian, Inc., Wallingford CT, 2009, 2016.

Table S1. Crystallographic data of **5**·$4CH_3CN$.

Compound	**5**·$4CH_3CN$
formula	$C_{94}H_{87}N_9B_2F_8P_8Pd_4$
formula wt	2189.78
cryst. syst	triclinic
space group	*P*1-
a, Å	14.5583(17)
b, Å	15.2367(14)
c, Å	23.782(3)
α, deg	96.5875(13)
β, deg	106.100(4)
γ, deg	106.649(4)
V, $Å^3$	4746.7(9)
Z	2
temp, °C	-120
D_{calcd}, g cm^{-1}	1.493
μ, mm^{-1} (Mo Kα)	0.943
2θ range, deg	6–55
R_{int}	0.021
no. of reflns collected	46478
no. of unique reflns	21290
no. of obsd reflns ($I > 2\sigma(I)$)	18861
no. of variables	1154
$R1^a$	0.037
$wR2^b$	0.097
GOF	1.068

[a] $R1 = \Sigma||F_o| - |F_c||/\Sigma|F_o|$ (for obsd. refs with $I > 2\sigma(I)$). [b] $wR2 = [\Sigma w(F_o^2$ –l refs).

Table S2. Selected bond distances (Å) and angles (º) of **5**.

Bond Distances (Å)

Pd(1)	Pd(2)	2.8899(3)	Pd(1)	P(1)	2.3244(6)
Pd(1)	P(5)	2.3309(8)	Pd(1)	C(1)	2.116(3)
Pd(1)	C(2)	2.122(2)	Pd(2)	Pd(3)	2.6802(3)
Pd(2)	P(2)	2.2735(8)	Pd(2)	P(6)	2.2667(8)
Pd(3)	Pd(4)	2.6001(3)	Pd(3)	P(3)	2.2954(7)
Pd(3)	P(7)	2.2834(7)	Pd(4)	P(4)	2.3399(6)
Pd(4)	P(8)	2.3453(6)	Pd(4)	N(5)	2.132(2)
N(1)	C(3)	1.148(5)	N(2)	C(4)	1.149(4)
N(3)	C(5)	1.139(4)	N(4)	C(6)	1.142(6)
N(5)	C(13)	1.126(4)	C(1)	C(2)	1.486(5)
C(1)	C(3)	1.442(4)	C(1)	C(4)	1.432(4)
C(2)	C(5)	1.421(4)	C(2)	C(6)	1.445(5)
C(13)	C(14)	1.452(6)			

Bond Angles (º)

Pd(2)	Pd(1)	P(1)	81.026(19)	Pd(2)	Pd(1)	P(5)	83.994(19)
Pd(2)	Pd(1)	C(1)	113.03(8)	Pd(2)	Pd(1)	C(2)	103.52(9)
P(1)	Pd(1)	P(5)	113.76(2)	P(1)	Pd(1)	C(1)	102.91(8)
P(1)	Pd(1)	C(2)	143.01(10)	P(5)	Pd(1)	C(1)	141.78(8)
P(5)	Pd(1)	C(2)	103.24(10)	C(1)	Pd(1)	C(2)	41.07(13)
Pd(1)	Pd(2)	Pd(3)	166.040(10)	Pd(1)	Pd(2)	P(2)	91.85(2)
Pd(1)	Pd(2)	P(6)	95.581(19)	Pd(3)	Pd(2)	P(2)	86.99(2)
Pd(3)	Pd(2)	P(6)	86.08(2)	P(2)	Pd(2)	P(6)	172.47(2)
Pd(2)	Pd(3)	Pd(4)	177.826(10)	Pd(2)	Pd(3)	P(3)	92.76(2)
Pd(2)	Pd(3)	P(7)	93.684(19)	Pd(4)	Pd(3)	P(3)	88.21(2)
Pd(4)	Pd(3)	P(7)	85.45(2)	P(3)	Pd(3)	P(7)	172.85(2)
Pd(3)	Pd(4)	P(4)	86.009(19)	Pd(3)	Pd(4)	P(8)	87.209(19)

Pd(3)	Pd(4)	N(5)	177.83(7)	P(4)	Pd(4)	P(8)	173.21(2)
P(4)	Pd(4)	N(5)	95.74(6)	P(8)	Pd(4)	N(5)	91.05(6)
Pd(4)	N(5)	C(13)	172.7(2)	Pd(1)	C(1)	C(2)	69.67(17)
Pd(1)	C(1)	C(3)	108.9(2)	Pd(1)	C(1)	C(4)	119.24(18)
C(2)	C(1)	C(3)	116.5(2)	C(2)	C(1)	C(4)	120.3(3)
C(3)	C(1)	C(4)	114.4(3)	Pd(1)	C(2)	C(1)	69.25(15)
Pd(1)	C(2)	C(5)	119.6(2)	Pd(1)	C(2)	C(6)	108.04(19)
C(1)	C(2)	C(5)	119.1(3)	C(1)	C(2)	C(6)	117.7(3)
C(5)	C(2)	C(6)	114.9(3)	N(1)	C(3)	C(1)	178.7(4)
N(2)	C(4)	C(1)	176.5(4)	N(3)	C(5)	C(2)	179.1(5)
N(4)	C(6)	C(2)	178.8(5)				

[a] See Figure S1 for atomic numbering scheme.

Table S3. Selected bond distances (Å) and angles (º) of $\mathbf{4}_{\mathbf{opt}}$ determined by DFT optimization.

Bond Distances (Å)							
Pd1	Pd2		2.944	Pd2	Pd3		2.752
Pd3	Pd4		2.696	Pd1	P1		2.356
Pd1	P5		2.364	Pd1	N1		2.182
Pd1	H1		1.520	Pd2	P2		2.311
Pd2	P6		2.299	Pd3	P3		2.317
Pd3	P7		2.319	Pd4	P4		2.367
Pd4	P8		2.359	Pd4	N2		2.246
Bond Angles (º)							
Pd1	Pd2	Pd3	167.98	Pd2	Pd3	Pd4	178.25
P1	Pd1	P5	162.38	P1	Pd1	N1	97.27
P1	Pd1	H1	81.75	P5	Pd1	N1	97.78
P5	Pd1	H1	83.43	Pd2	Pd1	N1	75.74
Pd2	Pd1	H1	105.58	N1	Pd1	H1	178.20
P2	Pd2	P5	172.41	P3	Pd3	P7	171.68
P4	Pd4	P8	172.76	Pd3	Pd4	N2	176.96

[a] See Figure 2 for atomic numbering scheme.

Table S4. Natural atomic charge (NAC) and Wiberg bond index (WBI) for the DFT optimized structure of $[Pd_4(H)(\textit{meso}\text{-dpmppm})_2(CH_3CN)_2]^{3+}$ (**4$_{opt}$**).

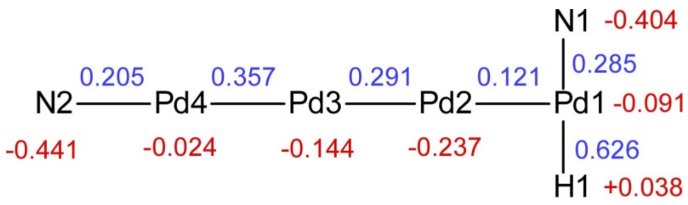

Atom	NAC	WBI			
		Pd1	Pd2	Pd3	Pd4
Pd1	-0.0912	0.0000	0.1207	0.0237	0.0138
Pd2	-0.2371	0.1207	0.0000	0.2914	0.1120
Pd3	-0.1439	0.0237	0.2914	0.0000	0.3569
Pd4	-0.0237	0.0138	0.1120	0.3569	0.0000
P1	1.1559	0.4860	0.0480	0.0034	0.0023
P2	1.0304	0.0265	0.3829	0.1064	0.0187
P3	1.0885	0.0035	0.0830	0.3893	0.1174
P4	1.0753	0.0033	0.0251	0.1290	0.3914
P5	1.1537	0.4854	0.0372	0.0020	0.0014
P6	1.0470	0.0356	0.3895	0.1049	0.0197
P7	1.0803	0.0038	0.0837	0.3856	0.1174
P8	1.0739	0.0036	0.0261	0.1292	0.3918
N2	-0.4406	0.0020	0.0164	0.0344	0.2050
N1	-0.4040	0.2852	0.0455	0.0029	0.0016
H1	0.0376	0.6255	0.0135	0.0017	0.0014

Table S5. TD-DFT calculations for the DFT optimized structure of $[Pd_4(H)($*meso*-dpmppm$)_2(CH_3CN)_2]^{3+}$ (**4**$_{opt}$).

Excited State 1:	Triplet-A	1.0506 eV	1180.07 nm	f=0.0000
387 -> 388	0.70743			
387 <- 388	0.16057			
Excited State 2:	Triplet-A	1.7683 eV	701.15 nm	f=0.0000
382 -> 388	0.15692			
383 -> 388	0.12872			
384 -> 388	-0.15251			
385 -> 388	0.24891			
386 -> 388	0.58165			
Excited State 3:	Triplet-A	1.8568 eV	667.72 nm	f=0.0000
383 -> 388	0.22153			
384 -> 388	0.57626			
385 -> 388	-0.22594			
386 -> 388	0.20430			
Excited State 4:	Singlet-A	2.0102 eV	616.77 nm	f=0.3698
383 -> 388	0.24535			
385 -> 388	0.11688			
387 -> 388	0.64415			
Excited State 5:	Singlet-A	2.1688 eV	571.68 nm	f=0.0016
382 -> 388	0.10835			
384 -> 388	-0.13793			
385 -> 388	0.18390			
386 -> 388	0.64097			
Excited State 6:	Singlet-A	2.2820 eV	543.32 nm	f=0.0093
383 -> 388	0.15268			
384 -> 388	0.50832			
385 -> 388	-0.39407			
386 -> 388	0.21294			

Figure S1. ORTEP views for the complex cation of **5**, $[Pd_4(tcne)(\textit{meso}\text{-dpmppm})_2(CH_3CN)]^{2+}$; (a) side and (b) top views. The ellipsoids are drawn at 40% probability level, and hydrogen atoms are omitted for clarity. Pd (violet), P (orange), N (blue), and C (gray).

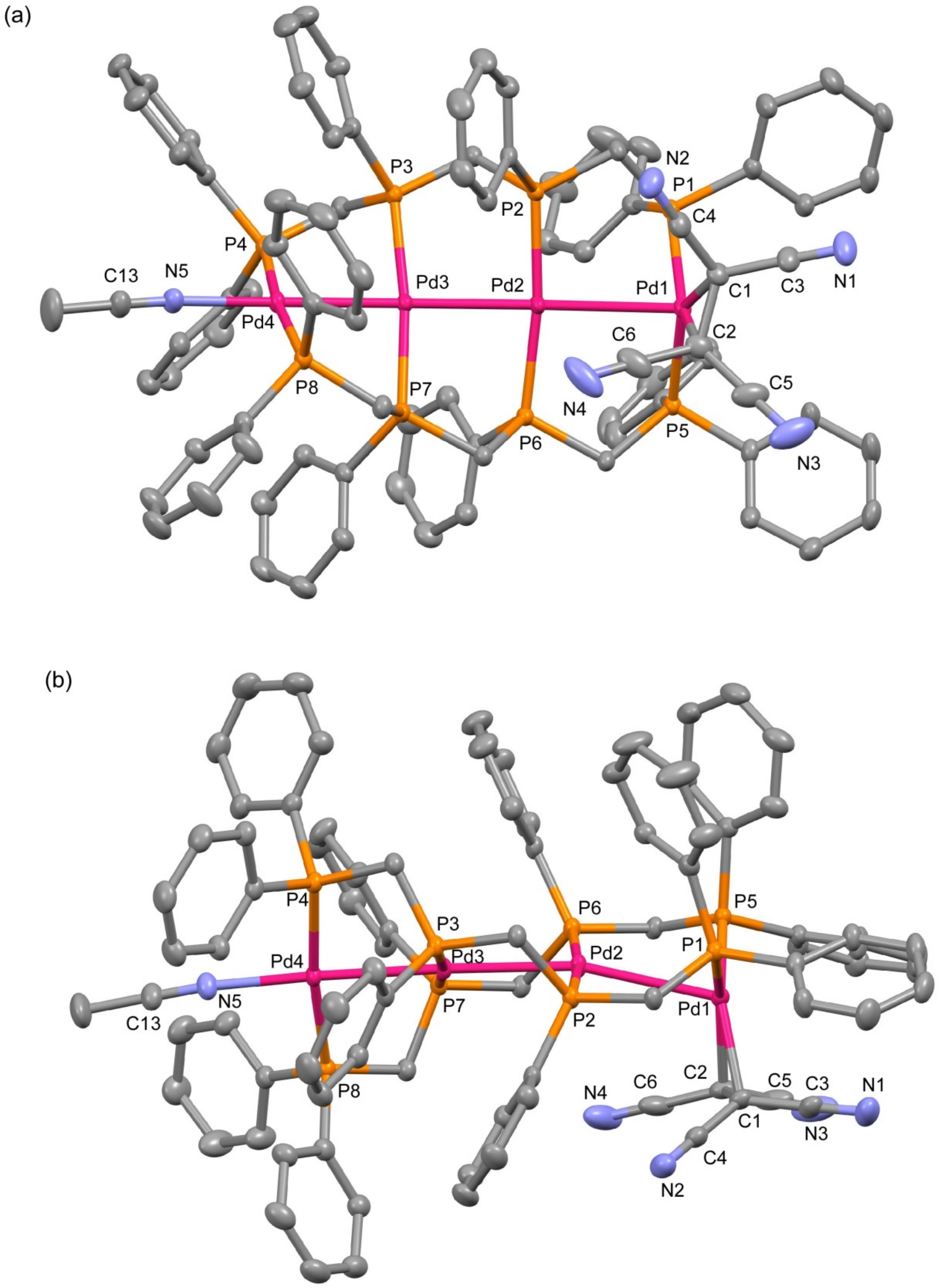

Figure S2. The DFT optimized structure for the complex cation of $[Pd_4(H)(\textit{meso}\text{-}dpmppm)_2(CH_3CN)_2]^{3+}$ ($\mathbf{4_{opt}}$), with LANL2DZ (for Pd), 6-311+G(d,p) (for hydride H), and 6-31G(d) (for others) basis sets, and IEFPCM (CH_3CN). The C–H hydrogen atoms are omitted for clarity. Pd (violet), P (orange), N (blue), C (gray), and hydride H (pink).

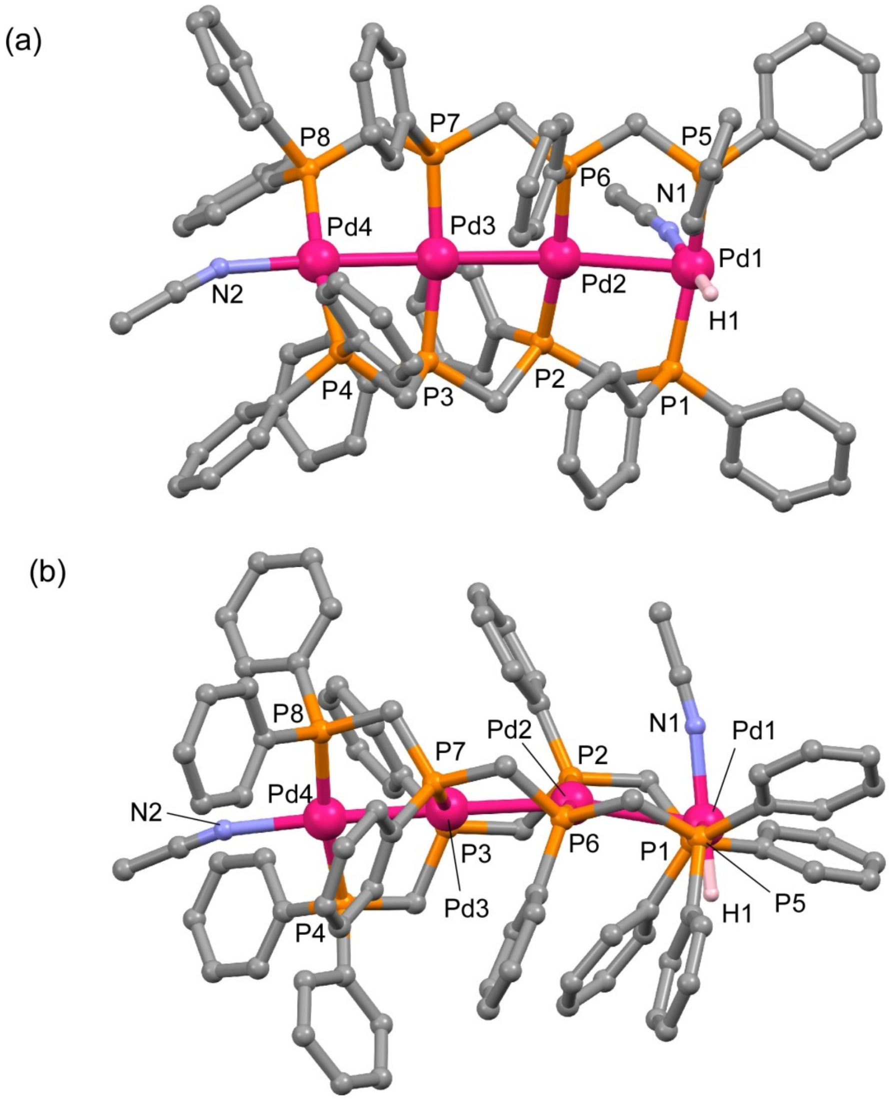

Figure S3. UV-vis-NIR spectral changes in CH_3CN for titration of $[Pd_8(\textit{meso}\text{-}dpmppm)_4(CH_3CN)_2](BF_4)_4$ (**1**) with successive addition of HBF_4 (portions of 0.2 eq.) at room temperature, forming **4** with the band maximum at 568 nm.

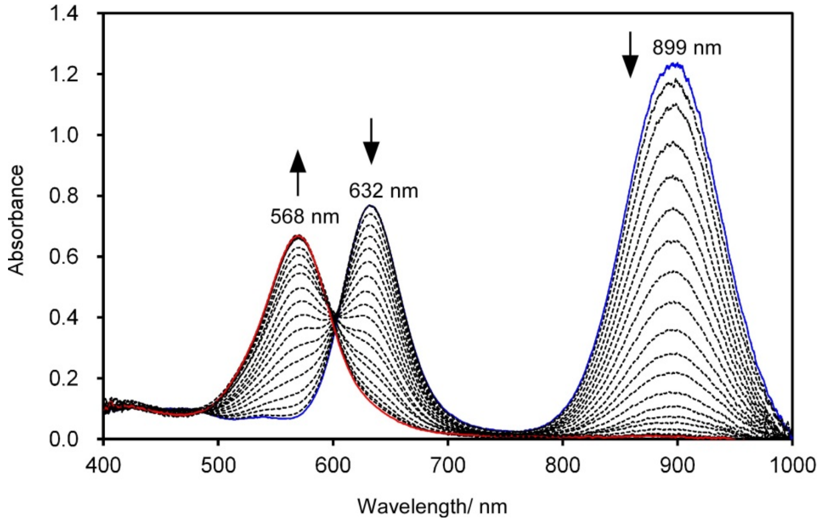

Figure S4. ESI mass spectra of **4** in CH_3CN at room temperature.

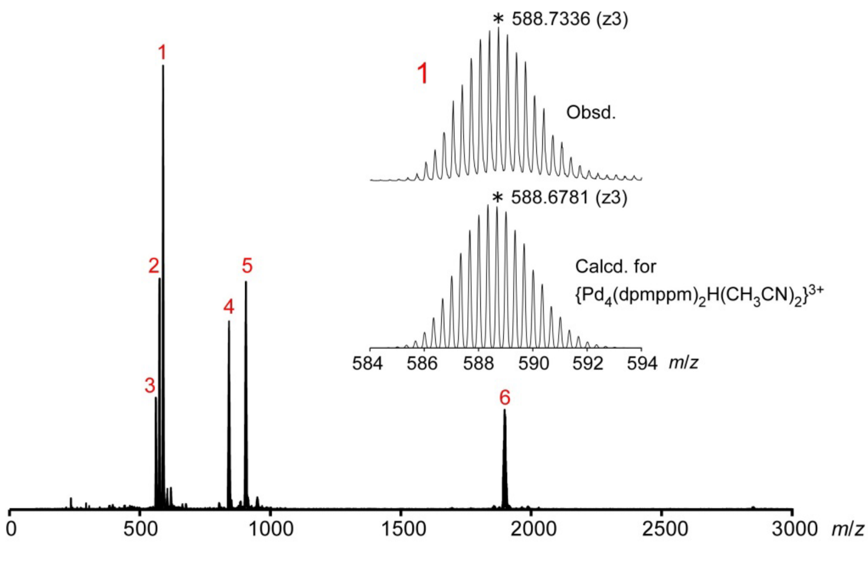

	Obsd.	Calcd.		Obsd.	Calcd.
2	561.0440 (z3)	560.9935 (z3) for $\{Pd_4(dpmppm)_2H\}^{3+}$	5	905.5975 (z2)	905.5055 (z2) for $\{[Pd_4(dpmppm)_2H(CH_3CN)_2]BF_4\}^{2+}$
3	574.7138 (z3)	574.6691 (z3) for $\{Pd_4(dpmppm)_2H(CH_3CN)\}^{3+}$	6	1898.2196 (z1)	1898.0146 (z1) for $\{[Pd_4(dpmppm)_2H(CH_3CN)_2](BF_4)\}^{+}$
4	841.5811 (z2)	841.4866 (z2) for $\{Pd_4(dpmppm)_2\}^{2+}$			

Figure S5. $^{31}P\{^1H\}$ NMR spectral changes in CD_3CN for the reactions of $[Pd_8(\textit{meso}\text{-dpmppm})_4(CH_3CN)_2](BF_4)_4$ (**1**) (●) with 0–4, eq. of HBF_4, showing the four resonances corresponding to **4** (●). The peak with * is impurity.

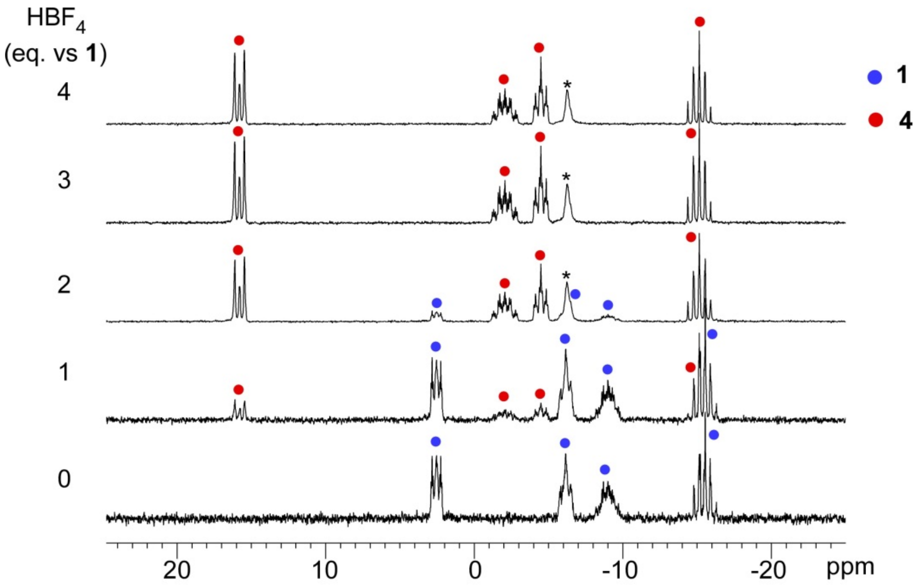

Figure S6. (a) $^1H\{^{31}P\}$ NMR of **1**, (b) $^1H\{^{31}P\}$and (c) $^{31}P\{^1H\}$ NMR spectra of **4** (generated from **1** with excess HBF_4 in situ) in CD_3CN at room temperature. * Impurity.

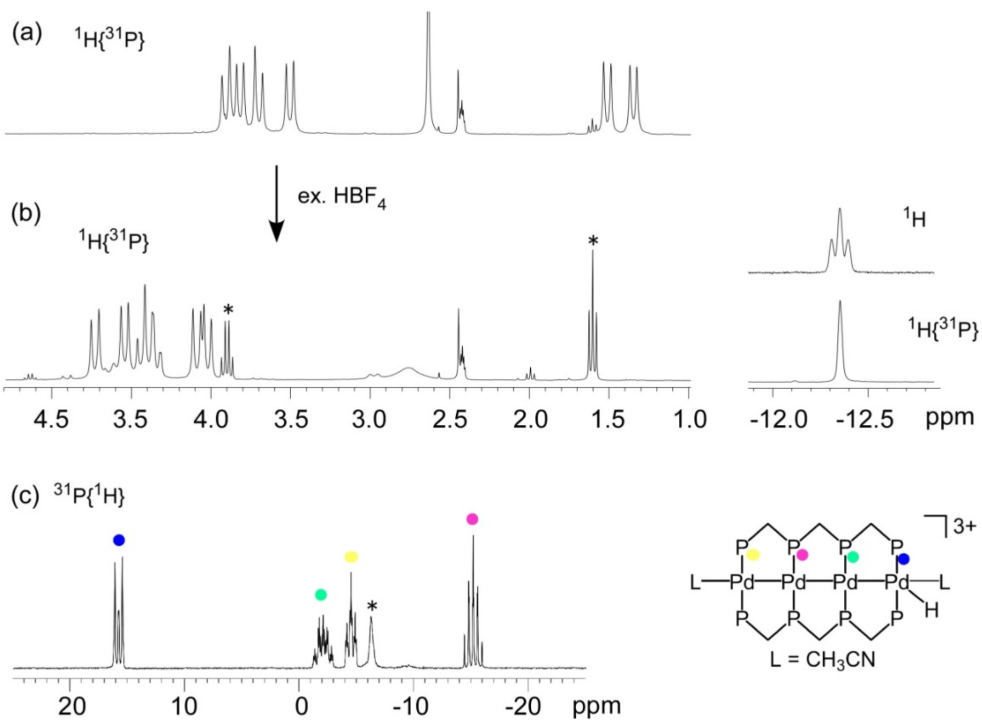

Figure S7. ^{31}P–^{31}P COSY (a) and ^{1}H–^{31}P HMBC (b) NMR spectra (121 MHz) of **4** (generated from **1** with excess HBF_4 in situ) in CD_3CN at room temperature.

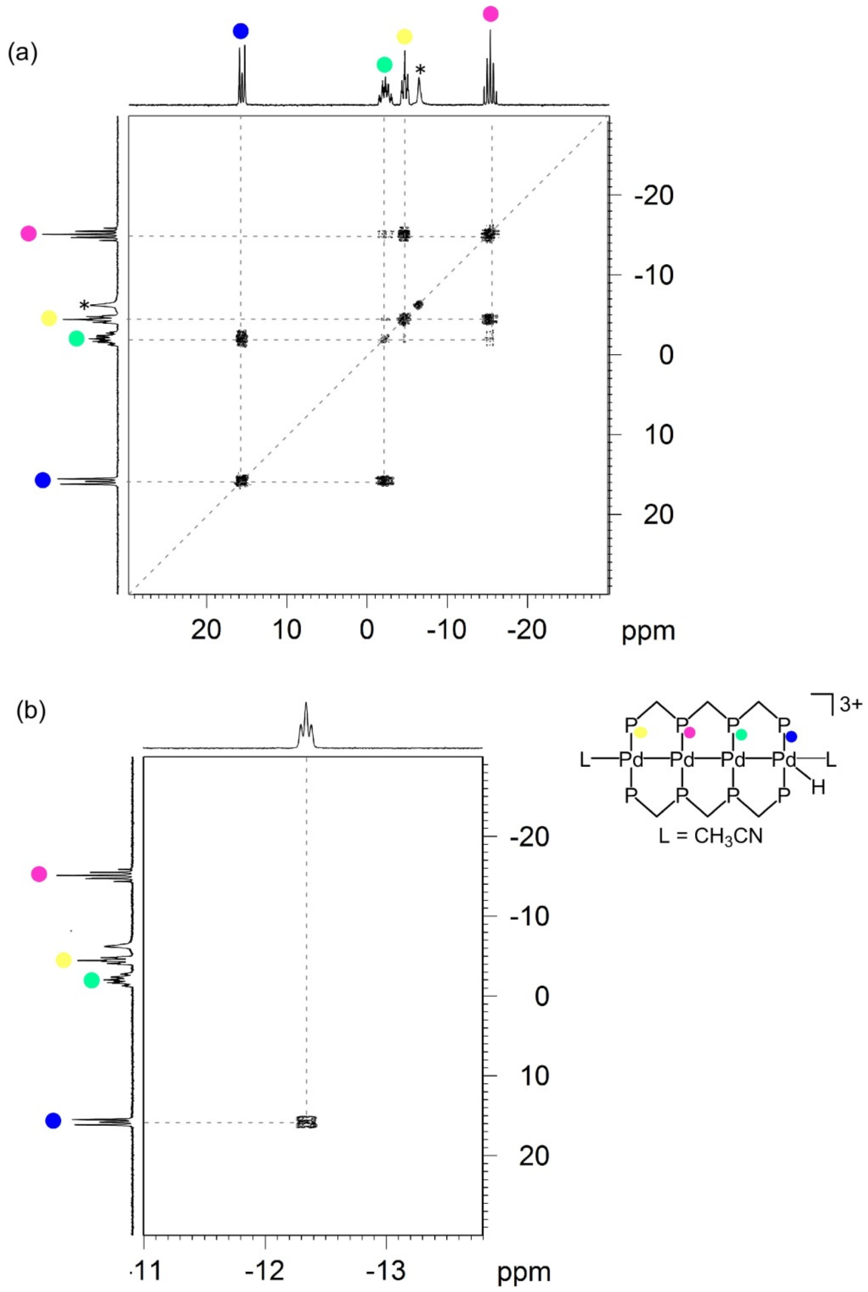

Figure S8. UV-vis absorption spectrum of **5** in CD_3CN at room temperature.

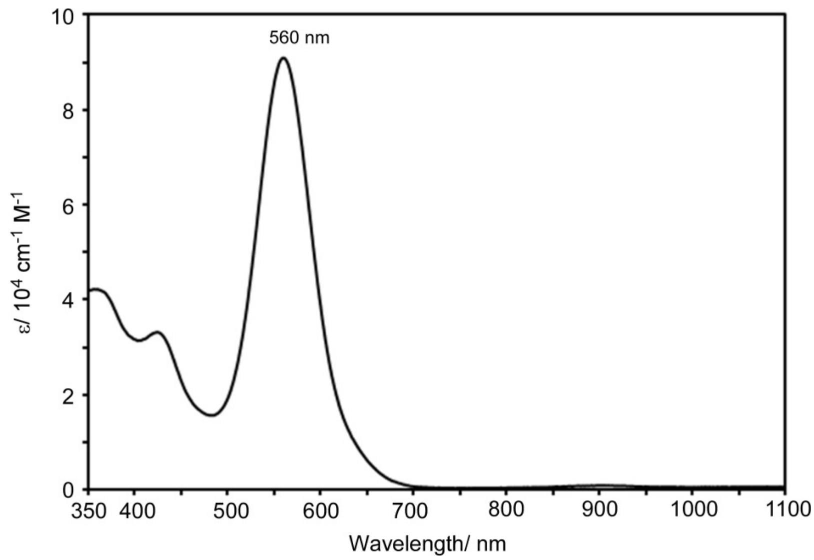

Figure S9. ESI mass spectra of **5** in CH_3CN at room temperature.

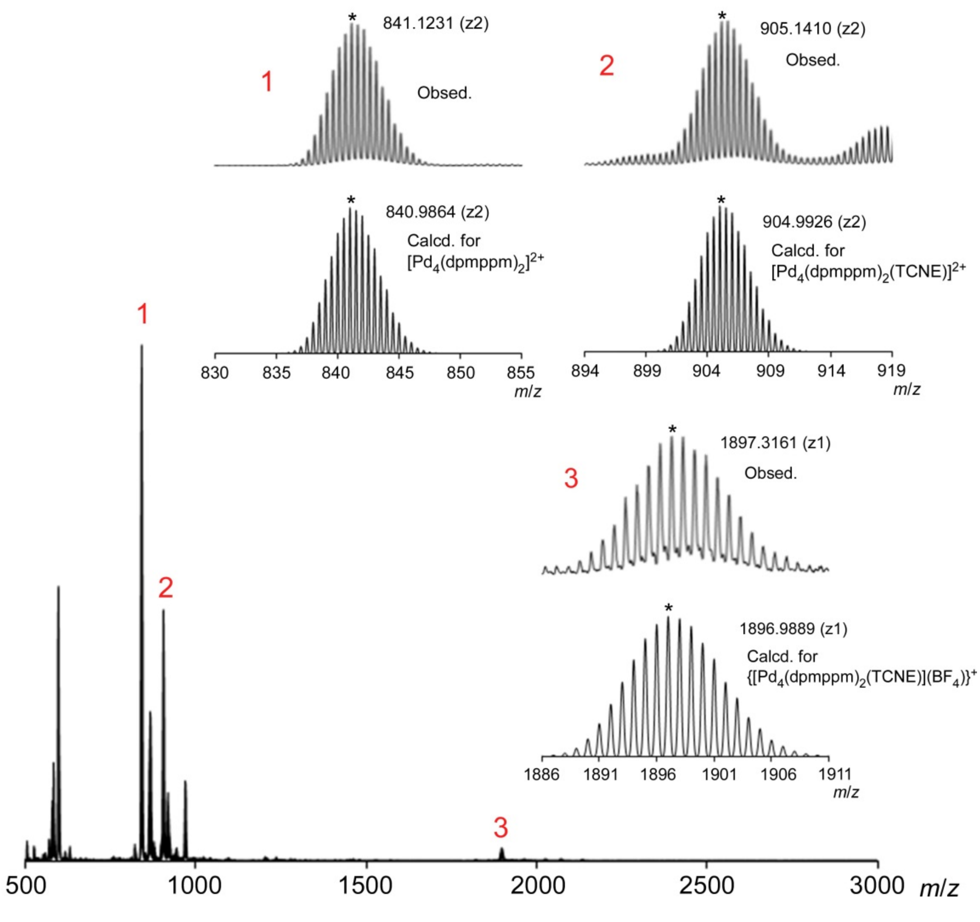

Figure S10. (a) $^{1}H\{^{31}P\}$, (b) $^{31}P\{^{1}H\}$, and (c) ^{31}P–^{31}P COSY NMR spectra of **5** in CD_3CN at room temperature.

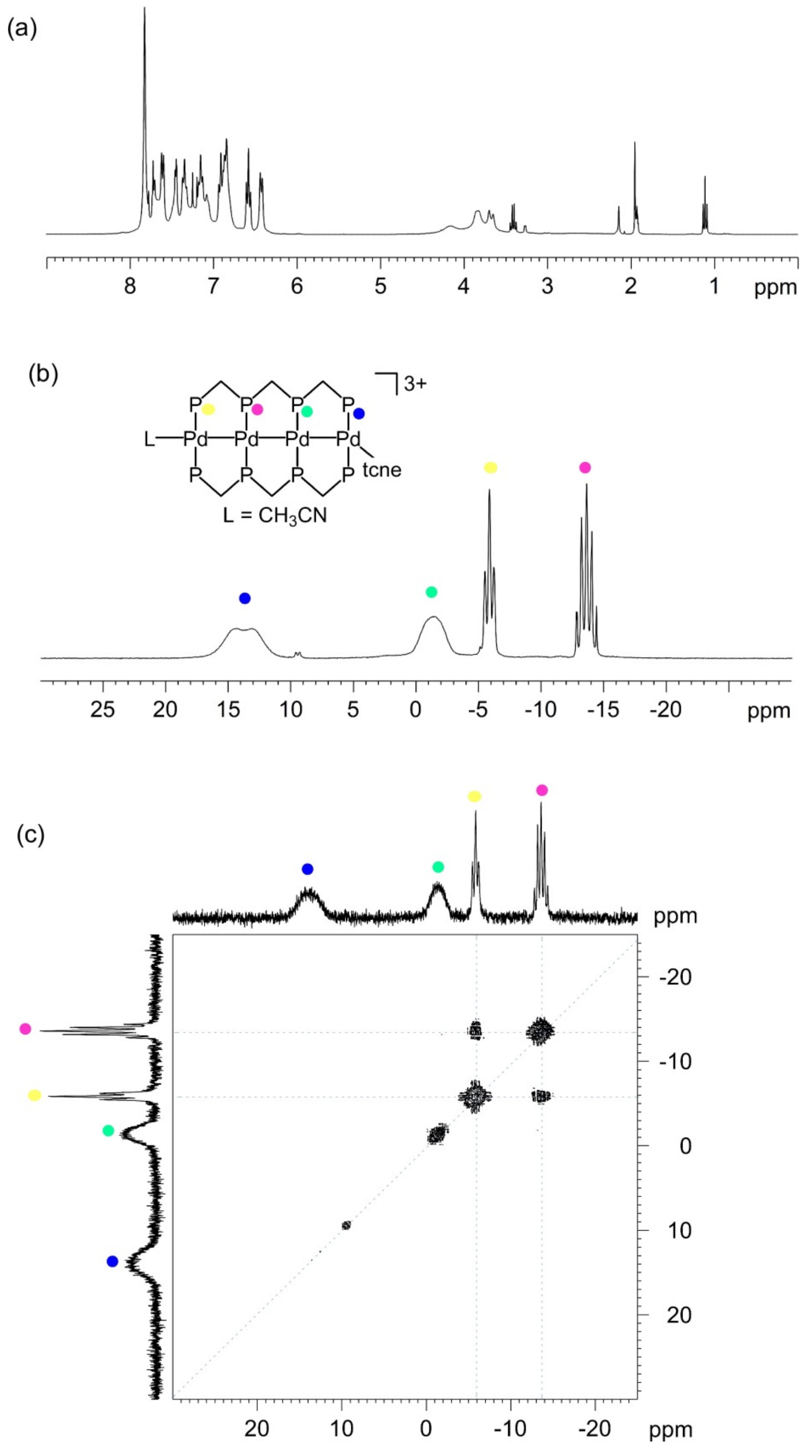

Figure S11. $^{31}P\{^1H\}$ NMR spectral changes of (a) **1**, (b) after addition of $HBF_4{\cdot}Et_2O$ (2 eq.), generating **4**, and (c) after further addition of Cp_2Co (4 eq.), restoring **1**, in CD_3CN at room temperature. The hydride (b) and hydrogen (c) peak were confirmed in ^1H NMR spectra at δ −12.3 and 4.6 ppm, respectively. *Impurity; It was not included in **1** and disappeared by the treatment with Cp_2Co, which might suggest that the peak corresponds to a small amount of by-product of hydride species, although the structure is not identified.

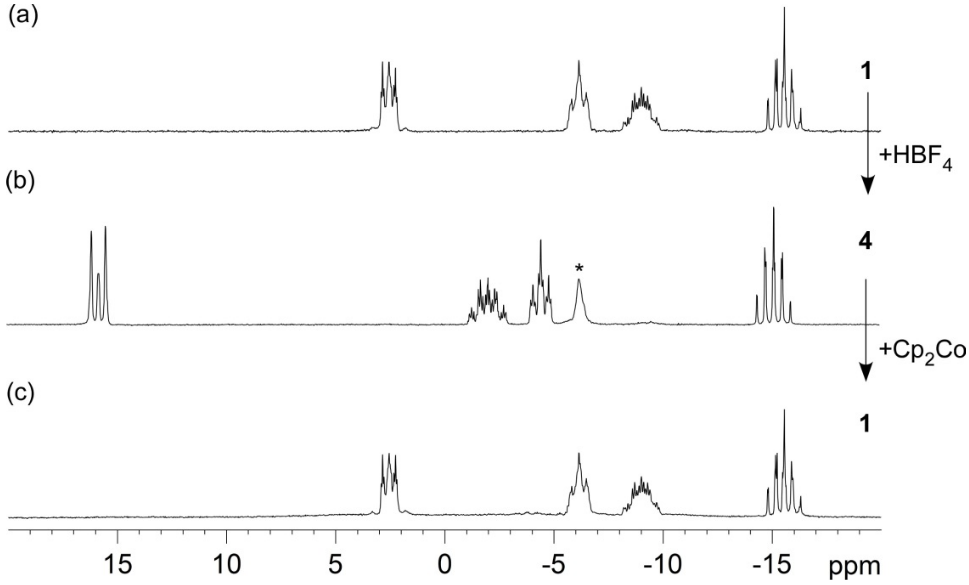

Figure S12. MO diagrams for $[Pd_4(H)(meso\text{-}dpmppm)_2(CH_3CN)_2]^{3+}$ (**4_{opt}**) derived from DFT calculations with B3LYP-D3BJ functionals and LANL2DZ (for Pd), 6-311+G(d,p) (for hydride H), and 6-31G(d) (for others), and IEFPCM(CH_3CN).

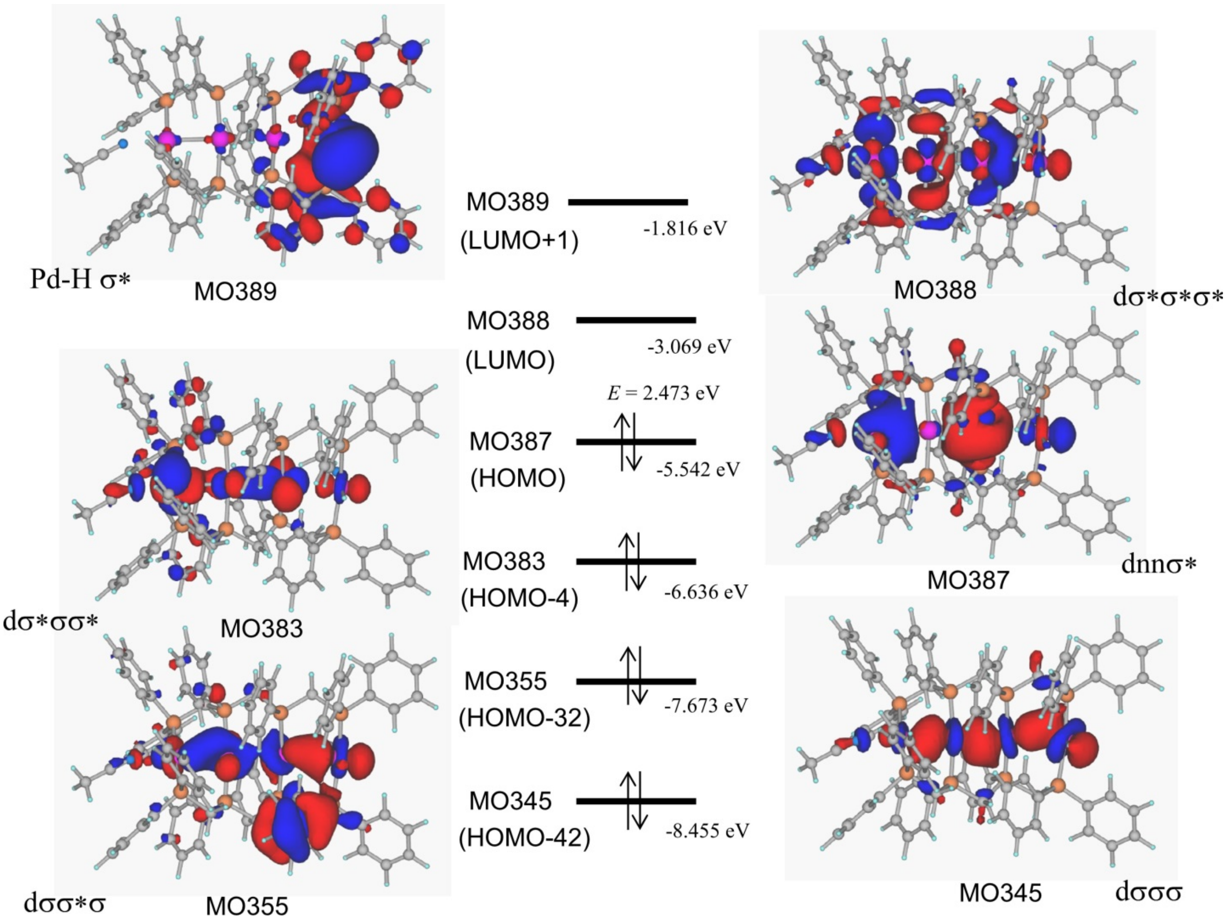

Figure S13. Cyclic voltammograms for 1 mM of **1** without HBF_4 (red line), with 2 eq. of HBF_4 (black line), and with 5 eq. of HBF_4 (blue line). Measured at room temperature with scan rate of 100 mV/s in CH_3CN containing 0.1 M [^{n}Bu$_4$N][BF$_4$].

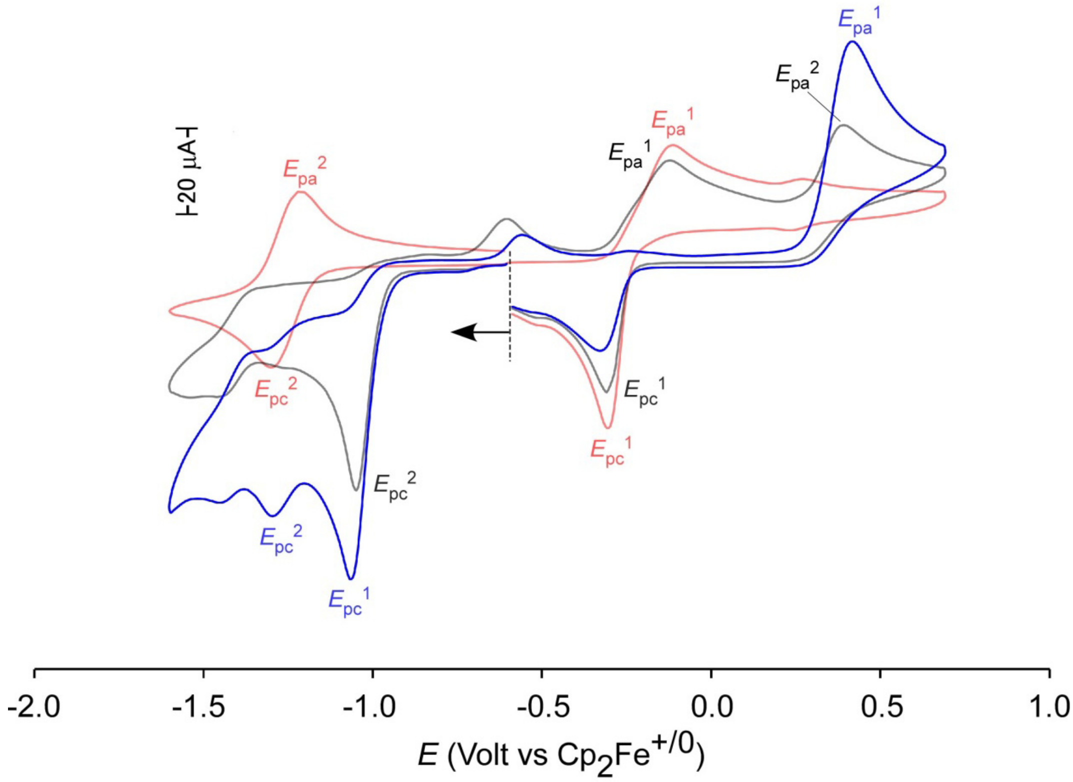

Figure S14. Cyclic voltammograms for 1 mM of **1** without HBF_4 (red line), with 2−10 eq. of HBF_4 (black and blue dotted lines), measured at room temperature with scan rate of 100 mV/s in CH_3CN containing 0.1 M [$^{n}Bu_4N$][BF_4].

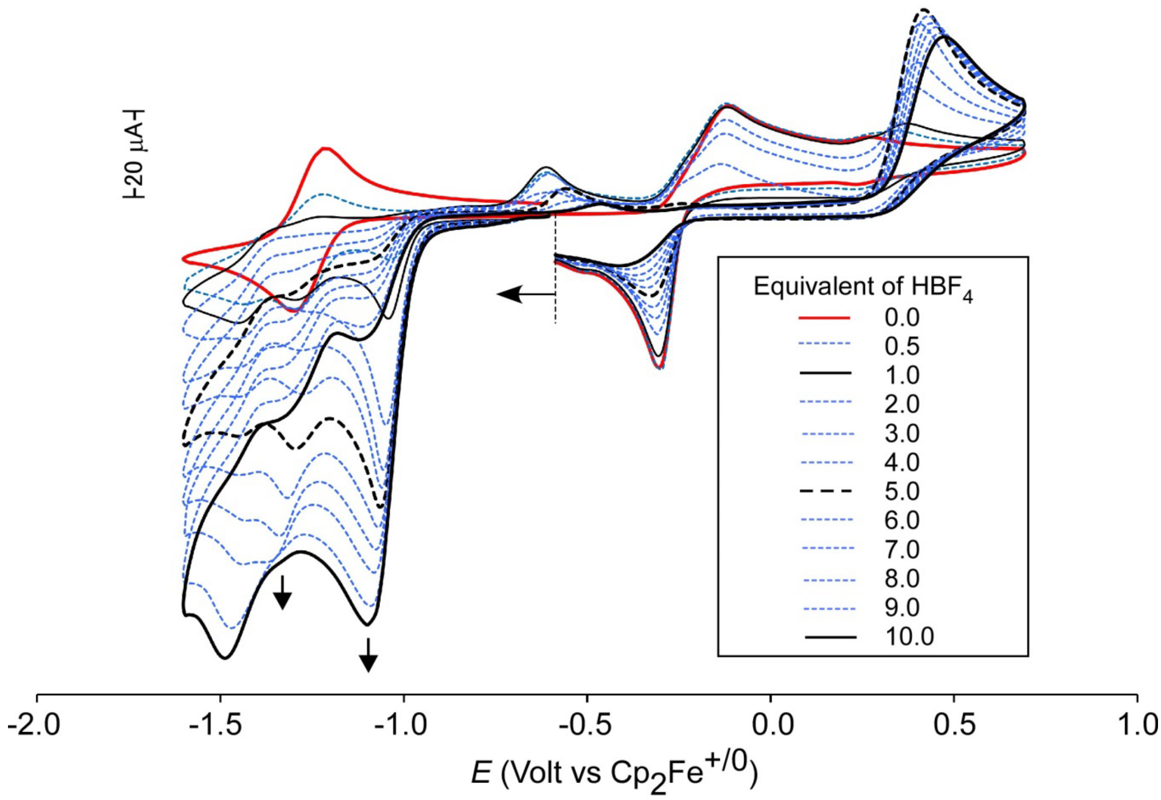

Figure S15. (a) Cyclic voltammograms for 1 mM of **1** without HBF_4 (red line), with 10−100 eq. of HBF_4, measured at room temperature with scan rate of 100 mV/s in CH_3CN containing 0.1 M [$^n Bu_4N$][BF_4] (left). A plot of I_{cat}/I_p vs $[H^+]^{1/2}$ (right). (b) CVs without **1** under the same conditions with HBF_4 (0–60 eq.), showing significantly weak reduction currents in comparison with those with **1**(a).

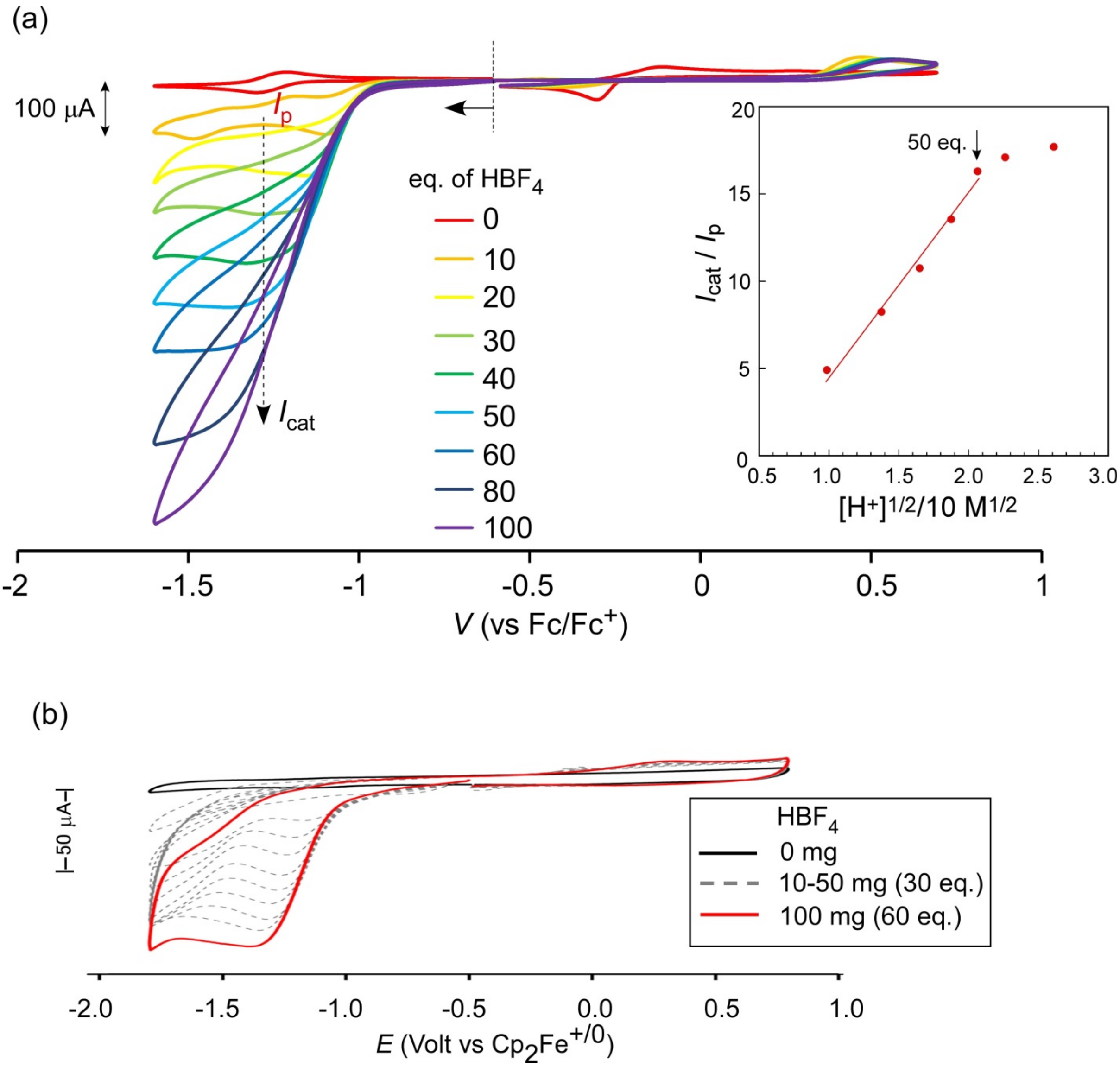

Figure S16. Repeating CV scans (−1.8 V to 0.8 V) by using glassy carbon electrodes (5 mmϕ) coated with Nafion membrane film containing (a) **1** and 1 eq. of BI (forming **3**), (b) **1**, and (c) without **1**, measured at room temperature with scan rate of 100 mV/s in CH_3CN containing 0.1 M [$^n Bu_4N$][BF_4].

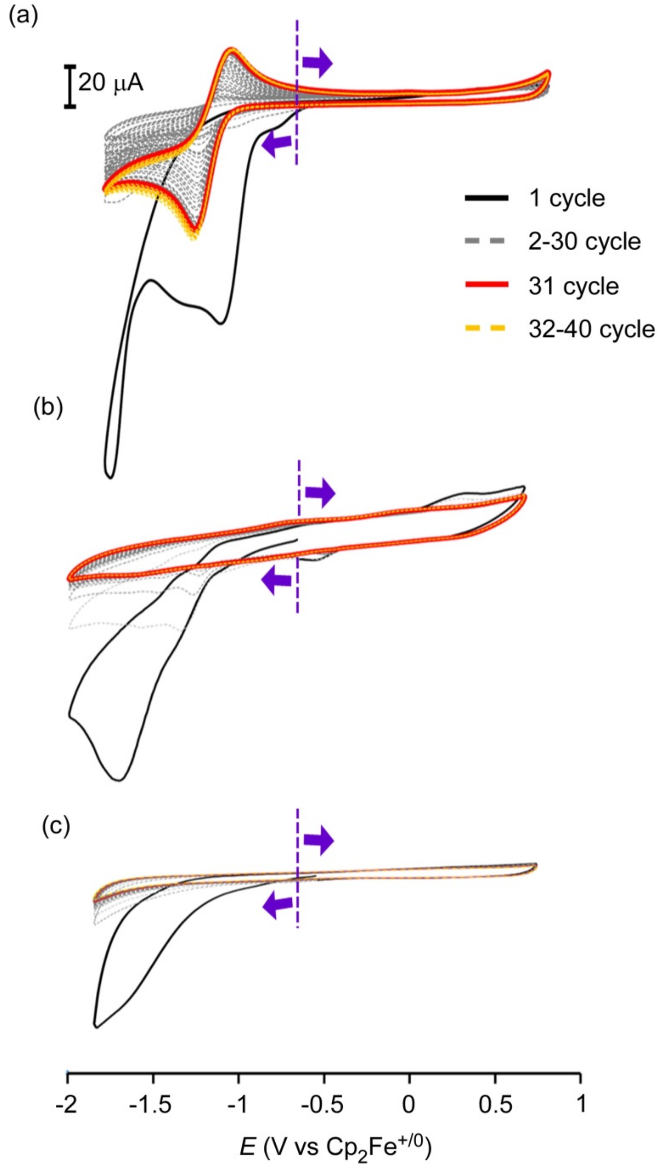

Figure S17. (a) Cyclic voltammogram with CMGCE/Nafion-**3**, , measured at room temperature with scan rate of 100 mV/s in CH_3CN containing 0.1 M [^{n}Bu$_4$N][BF$_4$] (left), (b) those with various scan rates from 50 to 1000 mV/s^{-1}, and (c) a plot of I_{pc} vs scan rate v/mVs^{-1}.

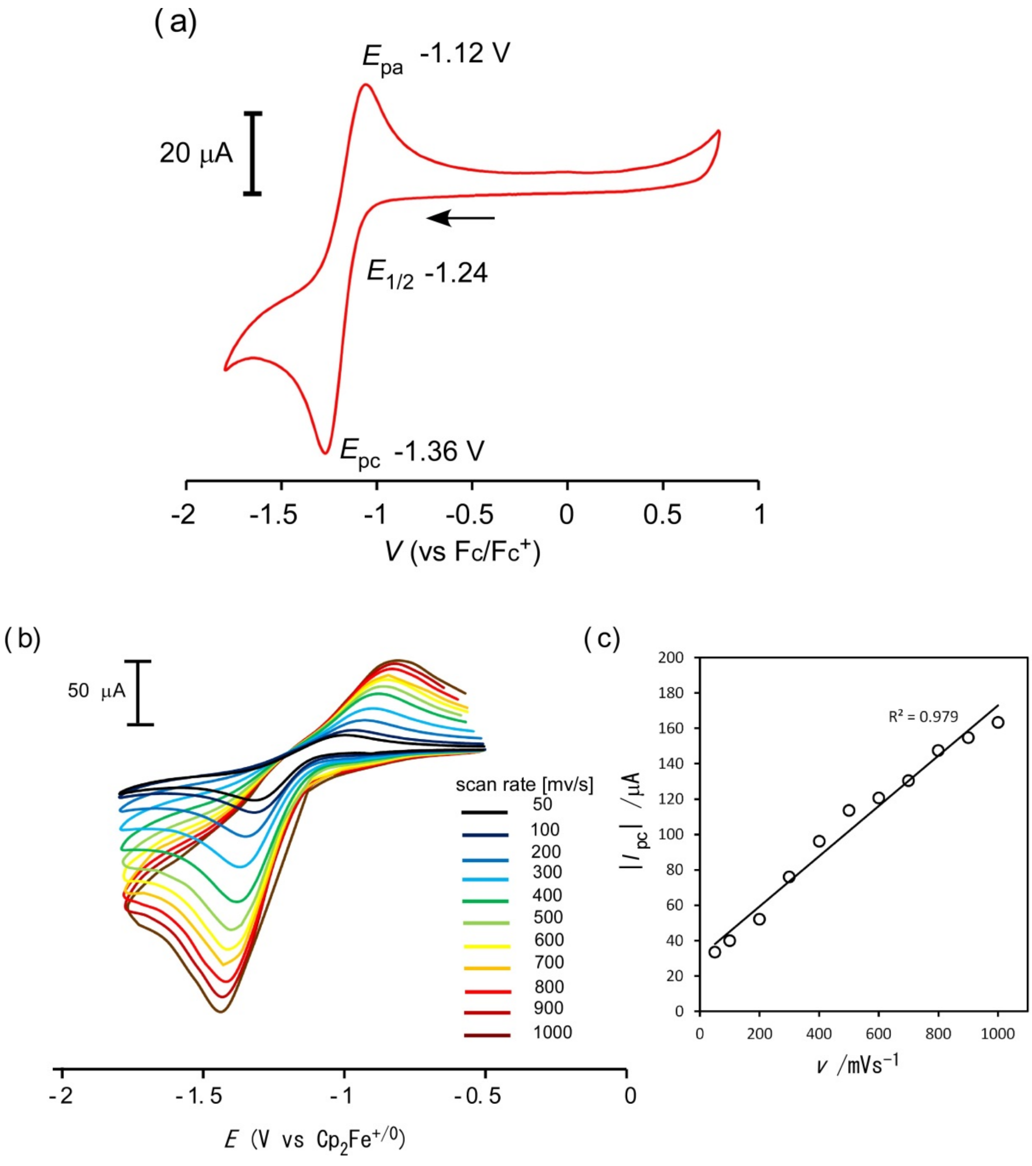

Figure S18. (a) Cyclic voltammograms with CMGCE/Nafion-**3**, in the presence of excess amounts of $HBF_4{\cdot}Et_2O$ (0-100 x 10^5 eq. vs **3**), measured at room temperature with scan rate of 100 mV/s in CH_3CN containing 0.1 M [^{n}Bu$_4$N][BF$_4$], and (b) a plot of i_{cat}/i_p vs ($[H^+]^{1/2}$)/mM$^{1/2}$.

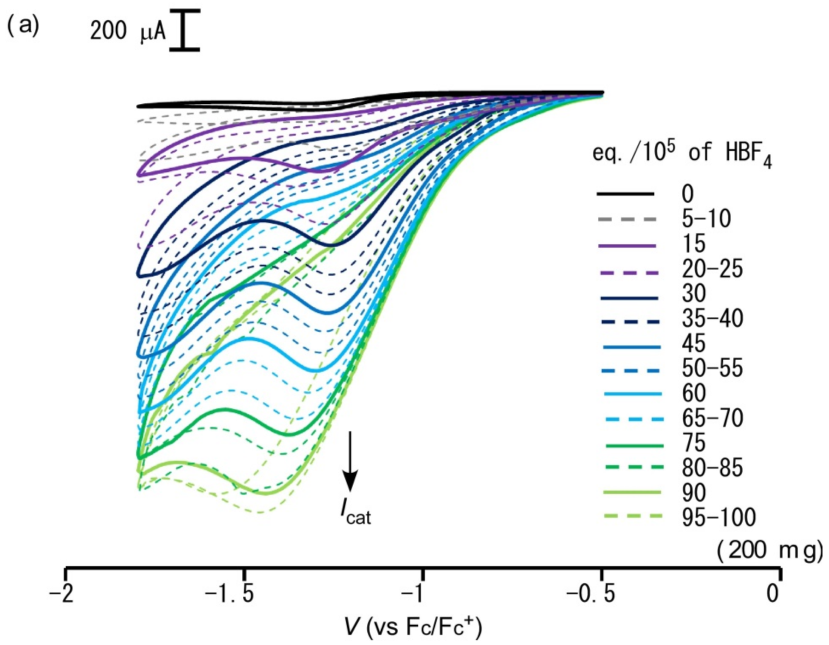

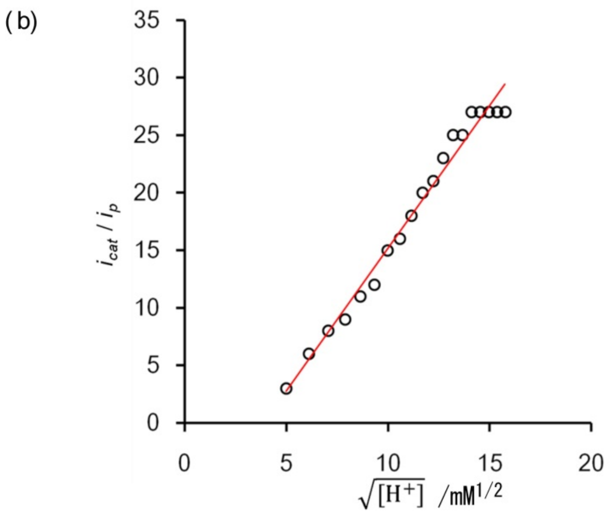

Figure S19. IR spectrum of $[Pd_4(H)(\textit{meso}\text{-dpmppm})_2(CH_3CN)_2](BF_4)_3$ (**4**) as KBr pellet.

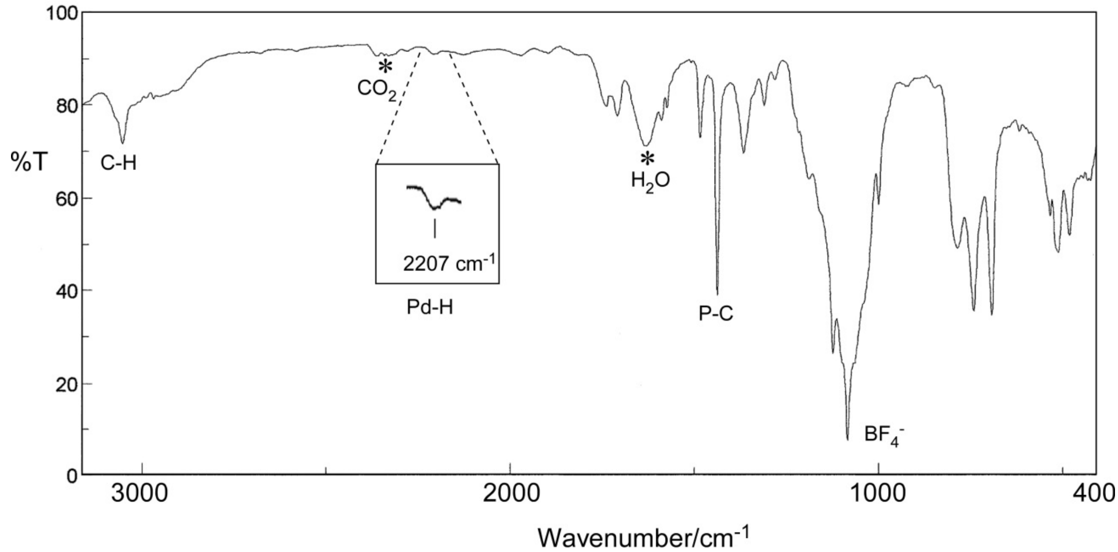

Table S6. Cartesian coordinates of the DFT optimized structure $\mathbf{4_{opt}}$.

Pd 0	4.692454	-0.389281	-0.287537
Pd 0	1.764444	-0.276059	-0.571077
Pd 0	-0.961728	-0.050080	-0.271582
Pd 0	-3.621954	0.182172	0.102235
P 0	4.229843	-2.511834	0.622137
P 0	1.460324	-2.566776	-0.568595
P 0	-1.174727	-2.168130	0.642416
P 0	-3.231661	-0.773546	2.231684
P 0	4.889964	1.951272	-0.561499
P 0	1.834341	2.012661	-0.768610
P 0	-1.047057	2.010502	-1.330730
P 0	-3.720720	1.088890	-2.073314
C 0	3.051832	-3.513258	-0.409359
C 0	0.380221	-3.161424	0.810285
C 0	-1.773796	-1.927829	2.364717
C 0	3.428475	2.649227	-1.463228
C 0	0.577894	2.618310	-1.988260
C 0	-2.111234	1.677834	-2.799160
C 0	5.684017	-3.568382	0.905096
C 0	6.900691	-2.929159	1.195811
C 0	8.043942	-3.683250	1.455792
C 0	7.985438	-5.078581	1.415190
C 0	6.781887	-5.718990	1.113287
C 0	5.632669	-4.969554	0.858450
C 0	3.334465	-2.392118	2.216761
C 0	2.696891	-1.190651	2.561346
C 0	1.876332	-1.125274	3.688683
C 0	1.693576	-2.258345	4.485251
C 0	2.343841	-3.452787	4.159073
C 0	3.161693	-3.521360	3.030497
C 0	0.590826	-3.214460	-2.036201
C 0	0.319954	-4.580213	-2.204406
C 0	-0.455250	-5.009458	-3.281028
C 0	-0.964903	-4.081501	-4.194607
C 0	-0.693086	-2.721432	-4.036895
C 0	0.081920	-2.287833	-2.960348
C 0	-2.364724	-3.296810	-0.144164
C 0	-2.657762	-4.539950	0.436804
C 0	-3.600347	-5.379728	-0.152985
C 0	-4.245932	-4.988517	-1.330665
C 0	-3.945058	-3.759603	-1.920685
C 0	-3.008399	-2.912611	-1.326609
C 0	-4.643443	-1.808264	2.768969
C 0	-5.230565	-2.669398	1.827219
C 0	-6.294427	-3.489381	2.197784
C 0	-6.794126	-3.443150	3.503137
C 0	-6.223723	-2.576043	4.437434
C 0	-5.148417	-1.760714	4.074189
C 0	-2.985310	0.463510	3.549456
C 0	-3.708018	1.664295	3.456553
C 0	-3.567123	2.646238	4.436454
C 0	-2.687246	2.451029	5.504252
C 0	-1.968159	1.258511	5.603948
C 0	-2.122578	0.263395	4.636700
C 0	6.337811	2.440285	-1.551820
C 0	7.522429	1.710009	-1.362807
C 0	8.672766	2.044784	-2.075174
C 0	8.645946	3.101412	-2.989544
C 0	7.467502	3.822834	-3.189799
C 0	6.314361	3.496526	-2.473870
C 0	4.911967	2.994650	0.941986
C 0	4.433238	2.498778	2.160543
C 0	4.308264	3.343148	3.263650
C 0	4.671303	4.686121	3.159590
C 0	5.166234	5.183694	1.951292
C 0	5.284164	4.344396	0.844786
C 0	1.449341	2.930861	0.758515
C 0	0.934532	2.199083	1.840628
C 0	0.535158	2.850048	3.007023
C 0	0.661711	4.236564	3.103918
C 0	1.185481	4.969804	2.034852
C 0	1.573922	4.322620	0.863141
C 0	-1.779494	3.466752	-0.524932
C 0	-2.135770	3.407946	0.826494
C 0	-2.688311	4.527413	1.448882
C 0	-2.900548	5.699130	0.721696
C 0	-2.553674	5.758199	-0.631748
C 0	-1.987908	4.647903	-1.253042
C 0	-4.779843	2.574240	-2.169918
C 0	-5.149013	3.234821	-0.992139
C 0	-5.892367	4.413685	-1.055385
C 0	-6.277566	4.930752	-2.293438
C 0	-5.918689	4.268752	-3.471971
C 0	-5.171817	3.093222	-3.412993
C 0	-4.424558	-0.078362	-3.287677
C 0	-3.805536	-0.404902	-4.500533
C 0	-4.393275	-1.336896	-5.359819
C 0	-5.607250	-1.935655	-5.021658
C 0	-6.235113	-1.604982	-3.816062
C 0	-5.643668	-0.690405	-2.947934
H 0	4.973685	-0.066570	1.170973
H 0	2.892168	-4.510455	0.009587
H 0	3.486673	-3.614600	-1.408071
H 0	0.194162	-4.238708	0.786079
H 0	0.847246	-2.902720	1.760430
H 0	-0.963747	-1.416491	2.891088
H 0	-2.014711	-2.850831	2.898411
H 0	3.468896	2.286478	-2.495825
H 0	3.462438	3.742928	-1.473338
H 0	0.776729	2.112965	-2.938857
H 0	0.595041	3.701273	-2.141726
H 0	-1.633822	0.849542	-3.330010
H 0	-2.239441	2.521750	-3.482740
H 0	6.948991	-1.843977	1.211693
H 0	8.980175	-3.181859	1.681079
H 0	8.877573	-5.665383	1.611422

H	0	6.734921	-6.802797	1.073576
H	0	4.708679	-5.484735	0.620067
H	0	2.819221	-0.318630	1.929483
H	0	1.384195	-0.191314	3.943188
H	0	1.051617	-2.210323	5.359527
H	0	2.210965	-4.332359	4.780962
H	0	3.657248	-4.454980	2.783754
H	0	0.696383	-5.308943	-1.492372
H	0	-0.670733	-6.066514	-3.402166
H	0	-1.578914	-4.419423	-5.023803
H	0	-1.096644	-1.997599	-4.737809
H	0	0.272833	-1.229723	-2.802968
H	0	-2.166533	-4.849827	1.354883
H	0	-3.833665	-6.335486	0.305879
H	0	-4.979015	-5.645442	-1.789153
H	0	-4.434712	-3.455575	-2.838939
H	0	-2.773122	-1.956509	-1.776795
H	0	-4.864716	-2.689336	0.806579
H	0	-6.738211	-4.156268	1.464920
H	0	-7.629574	-4.075504	3.787868
H	0	-6.612798	-2.532216	5.450163
H	0	-4.707678	-1.090682	4.804913
H	0	-4.374063	1.828701	2.615019
H	0	-4.138853	3.566184	4.363075
H	0	-2.567018	3.223206	6.257706
H	0	-1.291545	1.096050	6.437192
H	0	-1.575656	-0.666467	4.746350
H	0	7.537781	0.878795	-0.662671
H	0	9.585588	1.476986	-1.923230
H	0	9.540404	3.357830	-3.549013
H	0	7.442505	4.640559	-3.903472
H	0	5.406502	4.065808	-2.642454
H	0	4.143387	1.458270	2.245841
H	0	3.920071	2.950826	4.198140
H	0	4.571169	5.344257	4.017285
H	0	5.458390	6.226113	1.868931
H	0	5.668208	4.740610	-0.090208
H	0	0.828923	1.122017	1.749136
H	0	0.114990	2.278695	3.829463
H	0	0.350328	4.747802	4.009848
H	0	1.287623	6.047670	2.113000
H	0	1.972491	4.905193	0.038237
H	0	-1.976970	2.491392	1.381724
H	0	-2.947517	4.481529	2.500543
H	0	-3.336336	6.567330	1.206974
H	0	-2.727245	6.666062	-1.201001
H	0	-1.724230	4.699567	-2.305744
H	0	-4.835035	2.837669	-0.034452
H	0	-6.160898	4.929543	-0.138738
H	0	-6.855866	5.848598	-2.342939
H	0	-6.221321	4.668086	-4.435362
H	0	-4.896899	2.579584	-4.330020
H	0	-2.873007	0.064929	-4.791422
H	0	-3.902647	-1.586106	-6.295688
H	0	-6.063162	-2.657605	-5.692146
H	0	-7.177942	-2.070997	-3.546241
H	0	-6.121736	-0.453711	-2.002348
N	0	-5.825993	0.311102	0.513321
C	0	-6.824406	0.059828	1.044367
C	0	-8.058756	-0.280541	1.733226
H	0	-8.601016	0.629740	2.003486
H	0	-7.817509	-0.845102	2.639028
H	0	-8.687747	-0.896518	1.084586
N	0	4.334043	-0.900741	-2.379093
C	0	3.916076	-1.179633	-3.421010
C	0	3.358036	-1.538995	-4.714128
H	0	2.347092	-1.933728	-4.569646
H	0	3.980152	-2.302596	-5.189177
H	0	3.314196	-0.655868	-5.357648